

FAU

Friedrich A lexander U niversitat
Inst. T heor. P hys. III
Staudtstrasse 7
D -91058 E rlangen, G erm any

preprint FAU -T 3-94/1
hep-ph/9410254

The kinetic energy and and the geom etric structure
in the $B = 2$ sector of the Skym e m odel:
A study using the A tiyah-M anton A nsatz

N iels R .W alet

arXiv:hep-ph/9410254v1 10 Oct 1994

Subm itted to N uclear P hysics A

The kinetic energy and the geometric structure in the $B = 2$ sector of the Skyrme model: A study using the Atiyah-Manton Ansatz

Niels R. Walet

Institut für theoretische Physik III, Universität Erlangen-Nürnberg,
D-91058 Erlangen, Germany

March 26, 2022

Abstract

We study the construction of the collective-coordinate manifold in the baryon number two sector of the Skyrme model. To that end we use techniques of adiabatic large amplitude collective motion, which treat potential and kinetic energy on an equal footing. In this paper the starting point is the Ansatz proposed by Atiyah and Manton (Phys. Lett. 438B, 222 (1989)), which allows a study of the dynamics using a finite and small number of variables. From these variables we choose a subset of collective ones. We then study the behavior of inertial parameters along parts of the collective manifold, and study the dynamical parts of the interaction.

1 Introduction

In this paper we study an attempt to model the nuclear force from an underlying effective field theory, that mimics some aspects of the "correct" theory of strong interactions, namely QCD. This is in sharp contrast to the standard effective models of the nuclear interaction, which have been derived mainly through a description in terms of (virtual) meson exchanges. In general they have received remarkably little direct input from QCD (see Ref. [1] for a discussion of several approaches). Nevertheless such an approach is both a quantitative and qualitative success.

Another possible approach, which has only been pursued in recent years, is the use of models inspired by the large N_c limit of QCD [2, 3]. The prime example is the

electronic address: nwalet@theorie3.physik.uni-erlangen.de

Skyrme model [4], a non-linear theory of interacting pions, where baryons appear as topological defects – and this implements confinement. The model was conceived and forgotten in the early sixties, and was revived only in the early eighties by Witten and collaborators [5]. It has since been used successfully to describe the properties of baryons. Of course it was soon realized that one could use the model to describe baryon-baryon interactions as well [6, 7]. Actually even this idea seems to have been discovered by Skyrme [8].

The baryon-baryon interaction derived in this model was plagued by a lack of central attraction. In the early works the interaction was derived using the product approximation, which assumes that the two Skyrme ions do not deform as they approach. Furthermore one ignored the mixing between the nucleon and its excited states, which gives an attractive contribution to the central force. This question has recently been investigated in some detail, and it was found that the reintroduction of a finite number of colors (N_c), together with the use of a Born-Oppenheimer approximation is necessary to describe this part correctly [9, 10].

Apart from the static interaction (i.e., the part of the energy independent of velocities) there is a dynamical structure of the Hamiltonian as described by the kinetic energy. The inertial parameters are in general position dependent. If we use the fact that the mass tensor can be used as a natural metric on the configuration manifold, this shows that that coordinate space is curved. Actually little is known about these parameters. The only calculations have been performed using the product ansatz, and are thus only good for large separations. One of the important parts of the NN force, the spin-orbit interaction, derives purely from these kinetic terms. One finds that, even when the separation is large, and the product Ansatz is supposed to work, the sign of the spin-orbit force [11, 12, 13, 14, 15] does not agree with phenomenology. This problem has not yet been resolved.

The potential and kinetic energies can be derived from a knowledge of the solutions of the Skyrme model for finite separations. Unfortunately no such solutions exist. The best calculations up to date [16] calculate a set of fields obtained by imposing a constraint that is chosen in advance, and not determined self-consistently. As an alternative there exist the set of parametrized fields introduced by Atiyah and Manton [17]. These authors use an interesting technique to obtain a field of given topological quantum number from a parametrized instanton field. Its advantage is that the instantons, which are specified by a finite number of parameters, induce an effective Lagrangian for the Skyrme model depending on the instanton parameters. One can attempt to choose combinations among those that describe the collective manifold. As a first step towards this goal a calculation, similar in nature to that of Walhout and Wambach, of the static potential was performed by Hosaka et al [18]. This gave reasonable answers.

Since one can perform exact numerical solutions for the same problem, the greater promise of this Ansatz lies in the understanding of the geometrical structure of the collective manifold, which is closely tied to the kinetic energy. Atiyah and Manton

have recently [19] analyzed some aspects of this problem analytically. Several of the more quantitative aspects of this approach require numerical calculations, and cannot be resolved by analytical means. This paper is an attempt to study such an approach. There is a related idea to use the Atiyah-Manton Ansatz to study peripheral scattering [20]. Our work has no overlap with this approach, since we shall concentrate on short and intermediate distances. We believe that the long distance behavior can be best described by the product approximation, maybe suitably symmetrized.

The determination of collective coordinates in classical mechanics, or (equivalently) (time-dependent mean field theories, has been studied extensively over the past 20 years (see Ref. [21] for a discussion). As discussed in Ref. [21] the theory of adiabatic large amplitude collective motion (ALACM) is developed well enough to construct algorithms that are singularly well suited for this task. In this note we shall apply the AM Ansatz, and mix it with the notions of ALACM in order to study the structure of the adiabatic manifold. Similar calculations can be (and should be) performed by putting the Skyrme model on a grid. Since such a task is much more complex, both numerically and analytically, it is much harder to gain insight in that way.

The paper is organized as follows. In Sec. 2 we succinctly introduce the Skyrme model as well as the product Ansatz and the Atiyah-Manton Ansatz. In Sec. 3 we give a short introduction to the theory of Large Amplitude Collective Motion, as far as relevant for the current paper. In Sec. 4 we introduce the numerical techniques used in our calculations. In Sec. 5 we discuss the results of these calculations. Finally, in Sec. 6, we give a discussion and outlook. In three appendices we discuss which classes of solutions have a reflection symmetry, we give a detailed analysis of the fluctuations around the $B = 2$ hedgehog and we discuss the algorithm used in obtaining self-consistent solutions for the LACM equations.

2 Skyrme model and Atiyah-Manton Ansatz

2.1 The model

The "standard" Skyrme model is based on the non-linear sigma model, extended by a quartic interaction term and a pion mass term. The Atiyah-Manton Ansatz can only be used in the (chiral) limit of zero pion mass, where the model is defined by the Lagrange density

$$L = \frac{f^2}{4} \text{Tr}(\partial_\mu U \partial^\mu U^\dagger) + \frac{1}{32g^2} \text{Tr}[U^\dagger \partial_\mu U; U^\dagger \partial_\nu U][\partial_\mu U; \partial_\nu U]; \quad (1)$$

where U is a unitary two-by-two matrix-valued field satisfying the boundary condition $U = 1$ at infinity. As has been discussed many times before, this model has a topologically conserved quantum current. The charge of this current is identified with baryon

number B . Finally, one can also separate the U field in a pion field,

$$U = \frac{1}{f} (\sigma + i \vec{\tau} \cdot \vec{\pi}): \quad (2)$$

On occasion it may be useful to look at the vector pion field.

If we rescale the units of time and length, $x \rightarrow x/(gf)$, (the so-called Skyrme units), the Lagrange density takes on the slightly more convenient form

$$L = \frac{f}{g} \left[\frac{1}{4} \text{Tr}(\partial_\mu U \partial^\mu U^\dagger) + \frac{1}{32} \text{Tr}[U^\dagger \partial_\mu U; U^\dagger \partial_\nu U][\partial_\nu U; \partial_\mu U] \right]; \quad (3)$$

where f/g is the Skyrme unit of energy.¹ Finally the Skyrme Lagrangian can easily be reformulated in terms of the Sugawara variables (Lie-algebra valued currents) L_a ,

$$L = U^\dagger \partial_\mu U = i F_a^i; \quad (4)$$

and we have

$$L = \frac{1}{2} F_a^i F_a^i + \frac{1}{4} (F_a^i)^2 - \frac{1}{4} F_a^i F_b^i F_c^i F_c^i \quad (5)$$

2.2 Structure of the $B = 2$ manifold

Preliminary investigations of the structure of the $B = 2$ manifold have been performed in great detail using the product Ansatz, and are discussed in the reviews [22, 23].

Let us recapitulate the necessary details. For baryon number one the basic solution is the hedgehog,

$$U = \exp(i \hat{r} \cdot \hat{f}(r)); \quad (6)$$

with $f(0) = \pi$ and $f(\infty) = 0$. The baryon density has spherical symmetry, and the pion field points radially outward at each point of this surface. Actually one can perform a constant isorotation on the quantity U, U^\dagger , without changing the energy. This changes the direction of the pion field, and thus "grooms" the hedgehog.

One can use these solutions to construct the so-called product Ansatz. This uses the fact that the product of two U fields each with baryon number one, with arbitrary centers and grooming, has baryon number two. As Skyrme already understood, this Ansatz is only good at large separations. At smaller separations the two U fields no longer commute, and an asymmetry between the treatment of the two hedgehogs appears. Furthermore, the bound state in the $B = 2$ sector of the model, named "donut" after the toroidal symmetry of the baryon density [24, 25, 26, 27], can not be described by the product Ansatz.

¹There are many inequivalent definitions of the Skyrme units in the literature, depending on the definition of f . In our definition the S.J. of energy is equivalent to 11.18 MeV (for the "standard" values of $f = 54.1$ MeV and $g = 4.84$), and the S.J. of length is 0.754 fm.

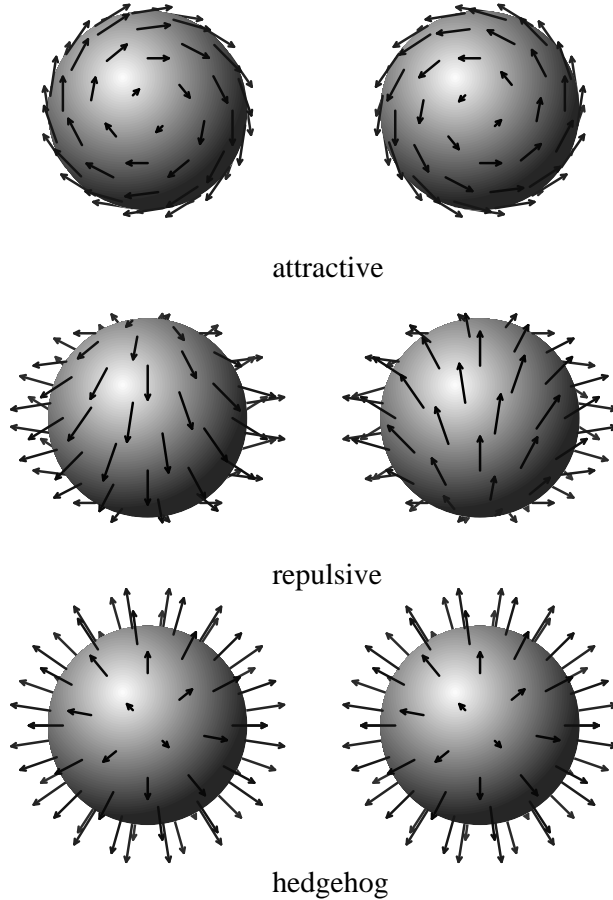


Figure 1: A schematic representation of the three channels, as they would appear in the limit of large separations. The spheres represent a surface of constant baryon density, and the arrows show the pion field on this surface. Here we have identified space and isotopic space.

One way out is to solve the Skyrme model numerically on a grid, with in position of the separation of the two Skyrmions. This approach has been taken by Wambach and his collaborators [16, 28]. Actually they never solve for all possible states of two Skyrmions, but limit themselves to a subset of configurations with definite symmetries under reflections, called the attractive, repulsive and hedgehog channels. These configurations are represented schematically, using the product Ansatz solutions in which they go over for large separations, in Fig. 1. (A similar study using the Atiyah-Manton Ansatz was performed in Ref. [18].)

The three channels are first of all the hedgehog channel, where we perform no rotation on the two hedgehogs. All states have the same reflection symmetries as a single baryon-number two hedgehog. Second is the repulsive channel, where we

perform a 90° rotation of each hedgehog (180° relative angle) around the axis through the centers of the hedgehog. This is called repulsive since there is a strong repulsion in this channel. Finally there is the attractive channel where each hedgehog is rotated by 90° degrees about an axis orthogonal to the line connecting the two centers.

From the caricatures of the pion field drawn here one can easily see that the fields have a certain symmetry under reflection in each of the three coordinate planes. These symmetries are discussed in greater detail in Appendix A. The idea is that these symmetries endow a special importance to these configurations, since they are at least stationary against small fluctuations breaking the symmetries.

2.3 Atiyah-Manton Ansatz

As discussed in [19] one can derive a Skyrme field from an instanton field by integrating the time component of the gauge potential,

$$U(\mathbf{x}) = CS^{-1} \exp \int_1^Z A_4(\mathbf{x}; t) dt C^{-1} \quad (7)$$

Here S is a constant matrix, chosen such that U decays to 1 at infinity, and C describes an overall gauging. For the current work, where we shall only consider C near the identity, it is convenient to parameterize

$$C = \exp(i\tilde{\alpha} \cdot \tilde{\alpha}): \quad (8)$$

For the Jackiw-Nohl-Rebbi (JNR) instanton of charge $k = 2$ we have [29]

$$A_4(\mathbf{x}; t) = \frac{i\tilde{r}}{2} \tilde{\alpha}; \quad = \frac{k+1}{k} \frac{1}{X_{1j}}; \quad (9)$$

and we should use $S = -I$, to obtain a field of baryon number $B = 2$.

In order to solve for the AM value of U we convert the integral (7) to the solution of a differential equation. First introduce

$$\tilde{U}(\mathbf{x}; \lambda) = CS^{-1} \exp \int_1^Z A_4(\mathbf{x}; t) dt C^{-1} \quad (10)$$

This function satisfies the differential equation

$$\partial \tilde{U}(\mathbf{x}; \lambda) = \tilde{U}(\mathbf{x}; \lambda) A_4(\mathbf{x}; \lambda); \quad (11)$$

with initial condition $\tilde{U}(\mathbf{x}; \lambda = 1) = S$. The function $U(\mathbf{x})$ is obtained as the limit for $\lambda \rightarrow 1$ of \tilde{U} . Actually we prefer to work with the Sugawara variables L , Eq. (4), so that the Lagrange density does not contain explicit derivatives. These can also be calculated as the large λ limit of a quantity $\tilde{\Gamma}$, which satisfies the differential equation

$$\partial \tilde{\Gamma}(\mathbf{x}; \lambda) = [A_4(\mathbf{x}; \lambda); \tilde{\Gamma}(\mathbf{x}; \lambda)] - \partial A_4(\mathbf{x}; \lambda); \quad (12)$$

Here the boundary condition is $\Gamma(\mathbf{x}; 1) = 0$. By differentiating the differential equations (12) we can obtain expressions for derivatives of L with respect to the instanton parameters X_1 and X_2 , which will be needed later.

The field U defined in Eq. (7) does not have an explicit time dependence. There is an implicit dependence, due to a possible variation of the instanton parameters as well as the unitary matrix C with time. Let us denote the parameters $f_1; X_1; \dots$ collectively by \mathbf{x} . We then have

$$L_0 = -U^Y \partial U - L; \quad (13)$$

If we substitute this in the Lagrangian we obtain the form

$$L = T - V; \quad (14)$$

with

$$V = \frac{1}{2} \sum_{ija} X_{ij}^a X_{ij}^a + \frac{1}{4} \sum_{ija} X_{ij}^a X_{ij}^a + \dots; \quad (15)$$

and

$$T = \frac{1}{2} \sum_{ija} \dot{X}_{ij}^a \dot{X}_{ij}^a; \quad (16)$$

$$B = \sum_a \dot{X}_{ij}^a \dot{X}_{ij}^a + 2 \sum_a \dot{X}_{ij}^a \dot{X}_{ij}^a + \dots; \quad (17)$$

The Lagrangian is quadratic in the time-derivatives due to the special nature of the Skyrme model. This also means that we have broken the Lorentz invariance of the original equations, so that (13) can only be used to describe adiabatic (small velocity) motion.

In the Atiyah-Manton Ansatz we have thus replaced the general matrix $U(\mathbf{x})$, with an infinite number of parameters, by a form parametrized by 18 parameters, $C U(\mathbf{x}; \mathbf{C})^Y$. (At each point we can extract at most 16 dynamical parameters, we can always form at least 2 spurious combinations. For the channels with additional symmetry discussed in this paper, we always find one more spurious combination.) Even these 15 or 16 dynamical variables are too much to describe the collective motion. We wish to study the behavior of the slowest modes among those appearing in (13). The techniques for such an approach, in the case that the Hamiltonian is quadratic in momenta, are well-developed [21]. In the next section we will recapitulate one of the possible mechanisms of solution, that will prove convenient in the current context.

Let us now enumerate those configurations, that will be relevant for the rest of the discussion. Here we closely follow [18],

1. Product Ansatz.

The choice $X_1; X_2; X_3$ describes a product Ansatz solution with centers at X_1 and X_3 . In this limit one finds

$$U(\mathbf{x}) = G_1^Y U_1(\mathbf{x} - X_1) G_1 G_3^Y U_1(\mathbf{x} - X_3) G_3; \quad (18)$$

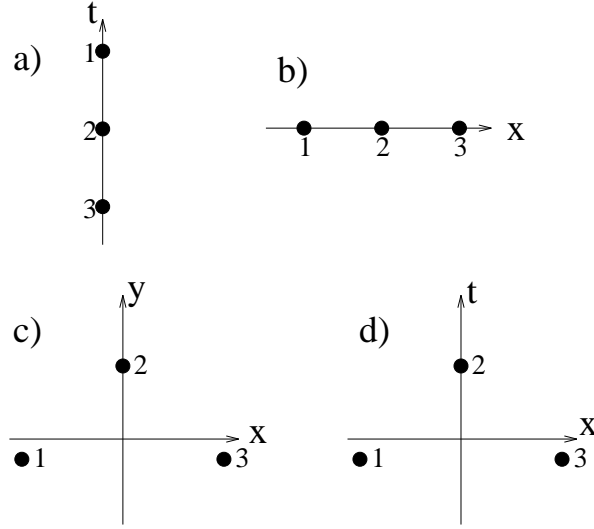


Figure 2: A schematic representations of the pole positions that describe the three channels in the Atiyah Manton Ansatz. The pole configuration a) represents a $B = 2$ hedgehog, b) states in the hedgehog-hedgehog channel. The triangle in c) represents the attractive states, and d) the repulsive states.

where the iso-rotational matrices G are given by

$$G_i = \frac{(T_i \quad T_2) + i(X_i \quad X_2)}{(T_i \quad T_2)^2 + (X_i \quad X_2)^2} \quad (19)$$

2. $B = 2$ hedgehog.

The hedgehog solution is found for the choice $x_1 = x_3 = 1$, $x_2 = 3/2$, $X_i = 0$, $T_1 = T_3 = 9/5$ and $T_2 = 0$.

3. The hedgehog channel.

In general states in the hedgehog channel are described by a pole configuration with all three poles on the x -axis, $x_1 = x_3 = 1$, $x_2 = 3/2$, $X_{11} = X_{31} = X$, $X_{21} = 0$, $X_{i(2;3)} = 0$, $T_i = 0$. The problem is that, even though the states in the hedgehog channel do have the same symmetry as the hedgehog, there is no continuous path from one to the other conserving the symmetry. The only common point, where we let the three poles coincide in the origin, corresponds to a state with $B = 0$. We shall turn to this problem in a future section, when we study the hedgehog numerically.

4. The attractive channel.

Here we have $x_1 = x_3 = 1$, $x_2 = 3/2$, $X_{11} = X_{31} = X$, $X_{12} = X_{32} = Y$, X_{22} free, all remaining components 0. Actually it was argued in [18] that a simple relation

between the parameter α_2 and the shape of the triangle (see below) describes the attractive channel best.

5. The repulsive channel.

Here we have the three poles aligned along the x-axis, $\alpha_1 = \alpha_3 = 1$, $\alpha_2 = \alpha$, $X_{11} = X_{31} = X$, $T_1 = T_3 = T$, T_2 free, all remaining components 0. Again the authors of Ref. [18] used the same relation as in the attractive channel between the shape of the triangle and α .

Let us use the ideas of [18] to study the configurations in the three channels. The authors of this paper use what can be called a turning-point approximation: At each point of the path they only consider the potential energy as if it were a stationary quantity. Of course this is only true if we tune the total energy at which we work to be equal to the potential energy. We thus end up in a turning point, since the kinetic energy has to be zero! Furthermore we can then use a virial argument to show that the quadratic and quartic terms in the Skyrme Lagrangian contribute in equal parts to the energy.

The formalism in the next section tries to improve on such an approach by including information about the kinetic energy. As a first guess the turning-point approach is fast and cheap. Let us look at the attractive and repulsive channel, and study the dependence of the energy on the form and weights of the triangles. The only remaining parameter, the size of the triangle, can be determined from a virial argument, since $E_2 = E_4$ at a stationary point. The hedgehog-hedgehog channel is of no special interest since it is specified by only two parameters, one of which follows from the virial argument. The remaining parameter then specifies the separation of the two solitons.

In order to study the energy we parameterize the triangles by introducing a second parameter T . In Ref. [18] it was assumed that this parameter equals w , the weight α_2 . The parameterization takes the form

$$\begin{aligned}
 \alpha_1 &= \alpha_3 = 1; \\
 \alpha_2 &= w; \\
 X_{11} &= \frac{q}{D = (1 - 1 = (1 + T)^2)}; \\
 X_{31} &= \frac{q}{D = (1 - 1 = (1 + T)^2)}; \\
 X_{12} &= D = (1 + T); \\
 X_{32} &= D = (1 + T); \\
 X_{22} &= D
 \end{aligned} \tag{20}$$

for the attractive channel. For the repulsive case X_2 should be exchanged with T . We now study the energy as a function of T and w for constant separation. The

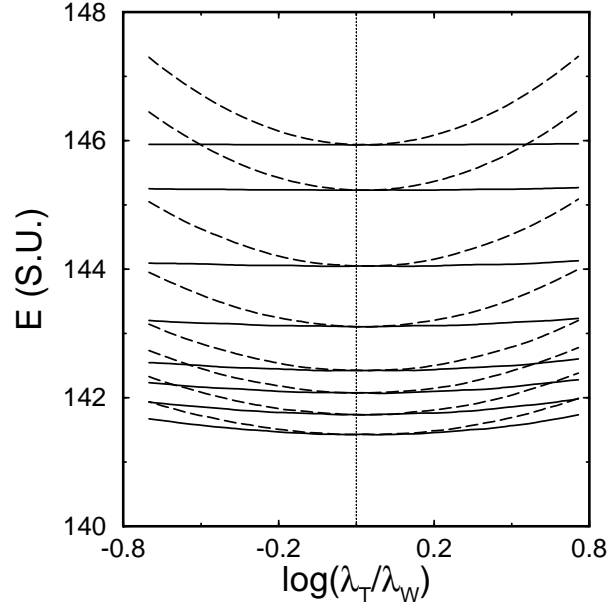


Figure 3: The energy at constant separation in the attractive channel as a function of $\log(\lambda_T/\lambda_W)$. From bottom to top the curves correspond to values of R of 1.2, 1.3, 1.4, 1.5, 1.7, 2.0, 2.5, 3.0 S.U. Dashed lines have $\lambda_T < 1$ and solid lines $\lambda_T > 1$.

The definition of separation is somewhat arbitrary. We use a rotationally invariant definition through the size of the quadrupole moment of the baryon-number distribution $(\int f(\mathbf{x}) d^3x B(\mathbf{x}) f(\mathbf{x}))$

$$R^4 = 4 \left(\frac{1}{3} (hx^2i^2 + hy^2i^2 + hz^2i^2 + hx^2ihy^2i + hx^2ihz^2i + hy^2ihz^2i + 3(hxyi^2 + hxzi^2 + hzyi^2)) \right) \quad (21)$$

The definition in Ref. [18] is based on the 11 component of the quadrupole tensor. As all sensible definitions should, both reduce to the separation between the centers of two isolated Skyrmions for large R .

In Fig. 3 we show the results for the attractive channel. Here the curves represent the energy at constant separation. It appears to be convenient to plot them as a function of $\log(\lambda_T/\lambda_W)$. We find two solutions of minimal energy for given R , both for $\lambda_T = \lambda_W$. This is due to the known inversion symmetry under $\lambda \rightarrow 1/\lambda$, where $\lambda > 1$ corresponds to separation along the x -axis, and $\lambda < 1$ to separation along the y -axis. (There may be a hint in our calculation that slightly unequal values of λ_T and λ_W may actually be the optimal solution, but that is probably due to a numerical inaccuracy.) A careful numerical study of the pion field suggests that the only solution with the requested mirror symmetries is the one with equal λ 's. Thus the valley in the energy for fixed separation corresponds to the equal values of λ as used in Ref. [18]. Of much

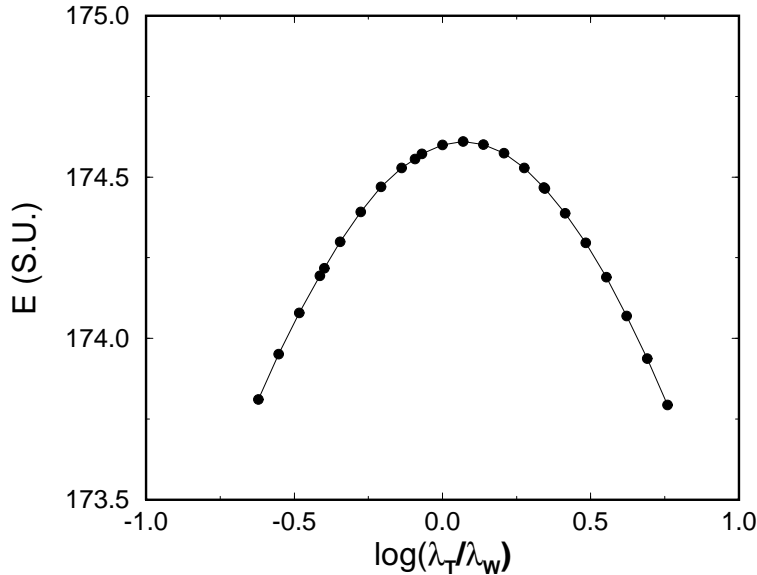


Figure 4: The energy at constant separation in the repulsive channel as a function of $\log(\lambda_T/\lambda_W)$. The value of R is 1:3 S.U.:

more interest is the repulsive channel, Fig. 4. A numerical study shows that only for $\lambda_T = \lambda_W$ we find the correct mirror symmetries for the repulsive channel. We have chosen to look at a small value of R , since only there the energy depends strongly on λ_T/λ_W , even though the same trend appears to persist for all R . Here we find that the energy is actually a maximum in the configuration with equal λ 's (and thus having the symmetries). This is not unexpected, since one would like to see that in the repulsive channel only those solutions most repulsive in nature appear.

3 Large amplitude collective motion

The approach used in selecting collective coordinates is discussed in detail in Ref. [21]. In this section we shall discuss the most important ingredients of that work, as well as the trivial transformation from a Hamiltonian to a Lagrangian formalism.

3.1 General Principles

Given a classical Lagrangian of a general quadratic form in time derivatives,

$$L = \frac{1}{2} \dot{B}^2 - V(B); \tag{22}$$

we look for those motions that are approximately decoupled. A decoupled surface is defined by the property that if we start the time-evolution from a point on the surface

(i.e., \mathbb{R}^2), with velocity – tangential to this surface, the motion remains on the manifold for all times. Since a slight perturbation of the Hamiltonian will destroy such a manifold, one sees that only very special models will have exact decoupling.

For that reason we look for approximate solutions. First of all, we select a subset of the exact decoupling conditions, that allows us to construct an algorithm to calculate a candidate manifold. Secondly we construct a decoupling measure, that allows us to gauge the quality of decoupling. This tells us whether it makes sense to consider the limited dynamics on the manifold.

Let us start with the first problem, which is the more complicated of the two. As is argued in Ref. [21], the mass matrix B actually plays the role of metric on the space q . We thus take over the standard notations of general relativity. In particular B with both indices raised is the inverse mass matrix. The geometric structure of the problem is especially clear in one of the algorithms useful in tackling the decoupling problem, the local harmonic approximation. This consists of the solution to the equations (the subscript i is a shorthand for the partial derivative $\partial = \partial_{x^i}$, ∂_i denotes the covariant derivative, to be defined below)

$$V_i = \sum_i^{X^i} f^{(i)}; \quad (23)$$

$$V_{i;j} B f^{(i)} = (f^{(i)})^2 f^{(i)}; \quad (24)$$

The first of these equations states that the force is parallel to an approximate set of tangent vectors to V , while the second equation is a local harmonic approximation (LHA) to the motion, which defines the approximate tangent vectors. Of great importance is the use of the covariant second derivative of V ,

$$\begin{aligned} V_{i;j} &= V_{i;j} - \Gamma_{ij}^k V_k \\ &= \frac{1}{2} B_{ij} (B_{ij} + B_{ji} - B_{ij}); \end{aligned} \quad (25)$$

We obtain the ordinary local harmonic approximation only at extrema of the potential energy ($V_i = 0$). At these points Eq. (23) is automatically satisfied. This allows for a path tracking approach, where we bootstrap from a stationary point.

Let us expand on this point, to clarify our approach. First note that since Eq. (24) is not a symmetric eigenvalue problem, we have independent left eigenvectors g_{ji} . With the standard normalization condition

$$g_{ji} f_i^j = \delta_{ij}; \quad (26)$$

these can be interpreted as defining the derivative of the old coordinates with respect to the new set which exhibits decoupling. The eigenvectors f then define the derivative of new with respect to the old coordinates. Suppose now that we start from a stable solution, in the case of the $B = 2$ Skyrme model that could be the donut or the

hedgehog. The direction in which we search are actually the least stable ones (the ones with the lowest harmonic frequency squared, $(\omega^{(i)})^2$) in Eq. (24). Suppose that we follow a single mode, as we will do in the next section. We then try to track a one-dimensional manifold by looking for a solution such that the RPA mode $g_{j,1}$ is an approximate tangent vector to the path. We thus take a small step in this direction,

$$= q_0 + g_{j,1} \quad (27)$$

In general this point does not lie on the path, i.e., it does not exactly satisfy the force condition (23), so that we have to look for a solution near this point. This is a non-linear problem, and can be solved in a variety of ways. In this work we use a very simple iterative method based on an approximate linearization of the force equations, as discussed in Appendix C. Once we have located a second point on this path, we proceed with the same steps sketched above. For the problem of the Skyrme ion, where we need to consider at least 6-dimensional dynamics to restore all the broken symmetries, we should actually calculate a many dimensional surface. We shall not pursue such an approach here, since it leads to significant topological and numerical complications, and shall concentrate on a small subset of the collective manifold instead.

Once we have found the coordinate surface, we define coordinate functions Q describing it, and we introduce

$$V(Q) = V(q); \quad (28)$$

and a collective mass B , equal to

$$B_{ij} = g_{j,1} B_{ij} g_{i,1}; \quad (29)$$

As usual for any linear eigenvalue problem, the scale of the eigenvectors is undetermined in Eq. (24). This freedom corresponds to a rescaling of the coordinates, which is always possible. Tensors are also transformed under such a rescaling. Of particular interest is the mass along the collective path, which can either be evaluated as

$$B_{11} = g_{j,1} B_{ij} g_{i,1}; \quad (30)$$

or as

$$B_{11} = \frac{\partial}{\partial q} B \frac{\partial}{\partial q}; \quad (31)$$

This last definition is based on the exact tangents to the decoupled manifold. Thus these definitions are only equal for exact decoupling. The normalized difference can be used to define a decoupling measure. If we normalize g such that $B_{ii} = 1$, we find that this decoupling measure can be cast in the suggestive form [30]

$$D = \sum_{i>2}^X (dq^i - dq^1)^2; \quad (32)$$

Here one can approximate the change in the new coordinates, dq^i , by a finite difference,

$$dq^i = \frac{f^i}{\dot{f}^i} ; \quad (33)$$

which indeed defines a change in the new coordinates. It is obvious that if all coordinates are independent from the first coordinate we have exact decoupling. The steps dq^1 can then be used to define a collective coordinate,

$$Q = \int_{\text{path}}^X dq^1 ; \quad (34)$$

3.2 Redundant coordinates

One important difference between the current problem and all the previous ones studied is the appearance of redundant coordinates. This is easily treated using the local harmonic approximation. The manifestation of redundant coordinates (that may change from point to point) is a zero eigenvalue of the mass matrix B , which is thus no longer invertible. But to calculate the covariant derivative we need this inverse! The solution is to only perform the matrix inversion in the subspace with non-zero eigenvalues, the resulting B^{-1} correctly eliminates these non-physical eigenvectors, including their derivatives, from the LHA equations (24). Here it is thus of utmost importance to use covariant derivatives, since the affine connection contains information about the change of the unphysical modes with a change of coordinates. For the present model, where the extra degrees of freedom can be eliminated explicitly, this procedure can easily be shown to give correct results. We have chosen to use the full set of degrees of freedom since it provides a sensitive test for the numerical accuracy and the correctness of our program.

4 Numerical techniques

From the previous sections one may notice that we need the spatial integration of the Lagrange density, and the second derivative of the potential energy as well as the first derivative of the mass. Since the potential energy depends on the current I_1^a , we need up to the second derivative of I_1^a with respect to t . For the derivative of the mass, where the mass itself depends on I_1^a and \dot{I}_1^a , we need additionally the derivative of I_1^a . We have chosen to write exact differential equation for all these quantities, so as not to lose too much accuracy on the outset. Thus we need to solve, at each point in space, a set of 1269 coupled differential equations. This is solved by first going to the variable $t = 2 \arctan(\tau)$, and integrating from $\tau = -1$ to 1 , using a highly efficient Runge-Kutta routine [31] to solve the initial value problem.

The spatial integral is decomposed into a radial integral and an integral over the surface of a sphere, which we deform to an ellipsoidal shape by multiplying each of

the major axes with a constant. The integral over the surface of the sphere was performed with an efficient non-product formula (see Ref. [32] for general references to such formulas), which also has at least tetrahedral symmetry. The relevant methods for the sphere are discussed in great detail in the Russian mathematical literature [33, 34, 35]. For the work reported here we use both an 85 point 15th order and a 110 point 17th order formula. These have proven adequate for the task.

The remaining radial integral is transformed to the finite interval $(-1;1)$ by the mapping $r = (r_0 - a)/(r_0 + a)$. We then perform a Gauss-Jacobi integration over r , using the weight function $(1 - r)^2(1 + r)^2$. This takes into account the exact large r behavior of the slowest decaying integrand, which is the quadratic contribution to the potential energy, as well as the r^2 behavior near the origin. Judging from the values we found for the baryon number, this procedure is highly accurate. (We found a value of 2 in at least six significant digits.) Since the integrands are much more spread out the accuracy of the RPA matrices is somewhat less, but we feel that we can control the numerics.

5 Results

5.1 Attractive channel

We start the application of the machinery discussed in the previous sections by studying the fluctuation around the minimum energy solution, the donut. In the AM Ansatz this state can be described by a configuration where all three poles have equal weight $w_i = 1$, and the poles themselves are located in an equilateral triangle, see Fig. 2c. We first study the harmonic modes around the donut. The eigenvalues and the eigenfunctions (g_i , the left eigenvectors of $V B^{-1}$ (Eq. (24), that describe the change of the old coordinates as we follow each of the modes over an infinitesimal distance), are represented graphically in Fig. 5.

There are eight zero-modes, out of a maximum of nine. These correspond to the translations in space, rotations in space and rotations in iso-space. One disappears due to the special cylindrical symmetry, $2I_3 + J_3 = 0$, of the donut. Let us discuss the zero-energy part of the spectrum first. The first and second mode form a pair, describing a rotation around the y and x axis, respectively. Since a rotation of the poles around these axes also generates an overall isorotation, these modes mix with an overall iso-rotation around the same axis to compensate for this effect. The third mode describes a translation in the z -direction. The fourth and fifth modes describe iso-rotations around the y and x axis. The sixth mode describes the effect of the remaining (iso)rotational symmetry around the z -axis, $I_3 - 2J_3$. Modes seven and eight are the translations along the x and y axes (slightly mixed).

In table 1 we list the masses of the zero-modes, when normalized in such a way that they describe the effect of the standard generators. One should notice that the mass

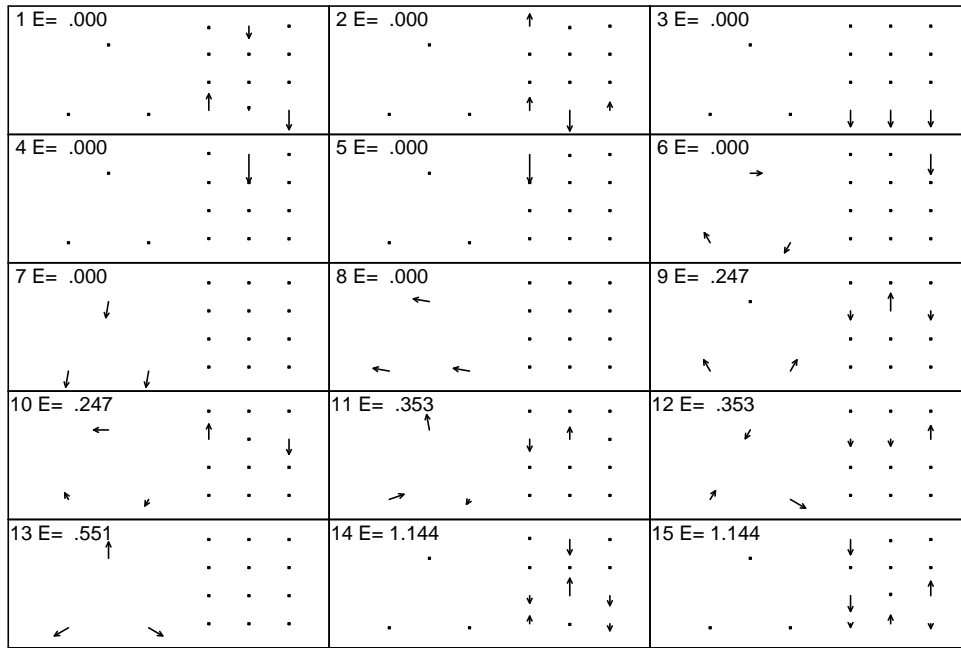


Figure 5: A schematic representations of the eigenvectors of the RPA problem around the donut. The arrows in each box denote the direction of the given component of the eigenvector. The triangle on the left gives the x,y components for each of the three poles. The triangle itself denotes the position of the poles. The four rows of three points on the right denote, from bottom to top, the z components, the time components and the change in \dots , for (from left to right) poles 1,2,3. The upper line gives the change in \dots (Eq. (8)).

Table 1: Masses of zero modes.

type of mode	mass (S.J.)
translation x	67.558
translation y	67.558
translation z	76.652
rotation x	86.964
rotation y	86.964
rotation z	130.342
isorotation x	57.258
isorotation y	57.258
isorotation z	32.585
o-diagonal z	65.171

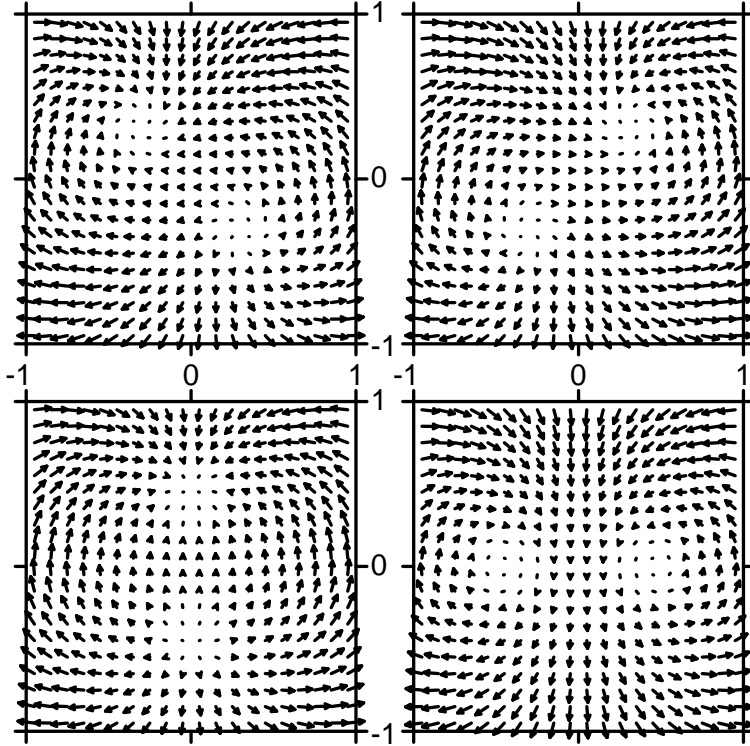


Figure 6: The pion field in the xy plane obtained by following the ninth (lowest two pictures) mode and the tenth mode (upper two) by a very small distance. We follow the modes in both positive and negative directions.

for translation is not completely isotropic. This is of course inconsistent with Galilei invariance, and appears to be incorrect. One can show that if the AM-donut were the minimum energy solution of the Skyrme equations this problem would not appear. It is due to the fact that the current Ansatz is not an exact stationary solution, and our covariant derivative, evaluated using the same Ansatz, can not correct for this effect. It shows some of the limitations of the present approach.

Now let us look at the finite energy modes. The ninth and tenth modes are the lowest energy ones, and should be the modes we are looking for. The simplest way to understand the meaning of these modes is to look at a plot of the pion field in the xy plane. In this plane the pion field has no z component, so we can plot it as an arrow in 2D space. Such a plot can be found in Fig. 6, where we have followed both these modes by adding and subtracting a small bit of the relevant mode vectors to the poles specifying the donut. The idea is that the pion field is only zero at the center of the donut, and that any perturbation will be clear from a change of the position of the zeroes. This is clearly the case! As one can see in the lower two figures, the ninth mode corresponds to the donut coming apart along either the x or y axis, the axis

depending on the sign of the mode eigenvector. The other mode corresponds to the system coming apart along an axis making an angle of 45° with the x and y axis. The reason is of course that the donut also has a reflection symmetry with respect to these axes! Actually the change in the pion field is trivial for these modes; it is a vector field parallel to the x or y axis, respectively.

The eleventh and twelfth modes are somewhat harder to understand. They look somewhat similar to the previous two modes, if we rotate the coordinate system by 45° . They are very different, however! The pion field changes in a complex and much less symmetric way than in the case of the previous modes. In general the trend seems to suggest that these modes may be those that connect to the hedgehog-hedgehog channel. The thirteenth mode obviously describes the breathing mode of the donut. Finally the last two modes describe a rotations in the time plane. Naively, as discussed in Appendix A this is another class of modes that are compatible with the reflection symmetries. These modes are pushed to a high energy due to a strong mixing with the isorotation C^∞ degrees of freedom. One might be tempted (as the author was) to forget about these global isorotations. This is not even approximately right, however, since without C^∞ these highest two RPA modes become the lowest in energy! For large distances a similar rotation in the time plane on two widely separated hedgehogs corresponds to a zero mode, i.e., in that case this mode does not change the energy of the system.

One of the main goals of the present work was to map out a path in configuration space where one follows the lowest mode, starting from the donut. This appears to be rather unproblematic (cf. discussions below), and there is no major obstacle. Some of the results are presented in Figs. 7-10.

In Fig. 7 we exhibit the diagonal inertial parameters for rotations, isorotations and translations (i.e., the mass) as a function of the coordinate Q . These show the expected (and not very exciting) behavior. The mass is almost constant since the energy is almost constant, and the breaking of Galilei invariance remains a minor nuisance. The moment of inertia for rotations increases drastically as Q increases, for rotations orthogonal to the axis of separation (x -axis). Parallel to this axis it decreases as expected. There is only one off-diagonal component in the inertia tensor. This is the z component of the term describing the mixing of the rotational and isorotational momenta. This term is almost constant. For the hedgehog it has to be there to remove the symmetry mode from the Hamiltonian. It appears to saturate at a value of about $73 S^2 U$ for large separations.

In Fig. 8 we show the decoupling parameter D , defined in Eq. (38). It is small, showing good decoupling. The discontinuity near $Q = 0.1$ is due to the fact that there the harmonic energy becomes zero, and we have mixing with the real zero modes, leading to slightly anomalous behavior. This is not important for the quality of the solution outside these points, since the conditions for a valley are local.

In Fig. 9 we show the potential energy V for movement in the attractive channel.

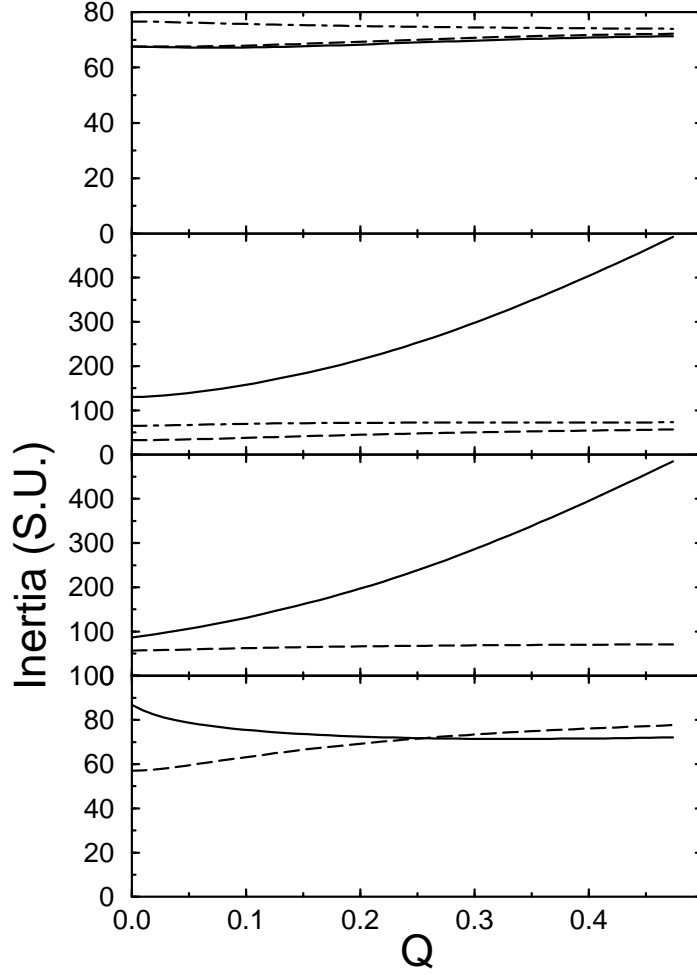


Figure 7: The inertial parameters in the attractive channel, obtained by following the lowest non-zero m mode from the donut. The lower three panels show the x , y and z components of the (iso)rotational moments of inertia (from bottom to top). Here solid lines represent rotational moments of inertia, dashed lines isorotational and dashed-dotted lines the off-diagonal component of the inertia tensor coupling the two. The upper panel shows the translational mass. The solid lines give the xx -, the dashed lines the yy - and the dashed-dotted lines the zz -component. Any component of the zero-mode inertia-tensor not shown is identically zero. Q is defined in Eq. (34).

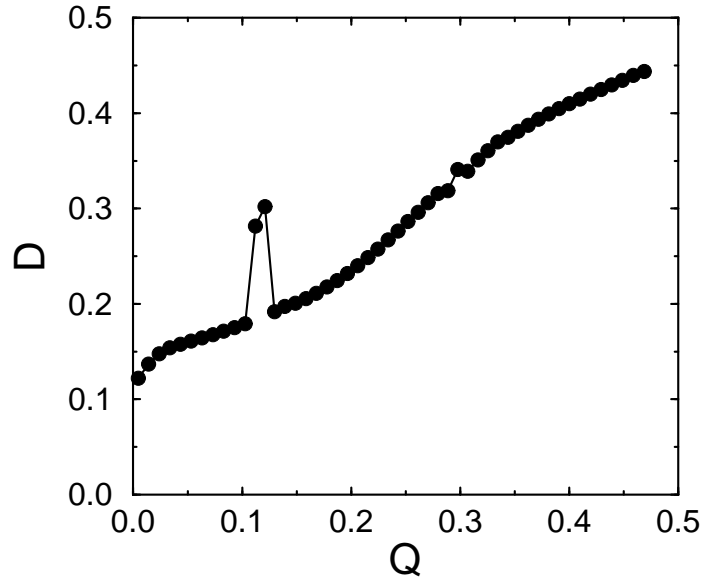


Figure 8: The decoupling measure D , Eq. (38), in the attractive channel, obtained by following the lowest mode. Q is defined in Eq. (34). The violent jump is due to poor convergence when the RPA frequency of the mode followed goes through zero.

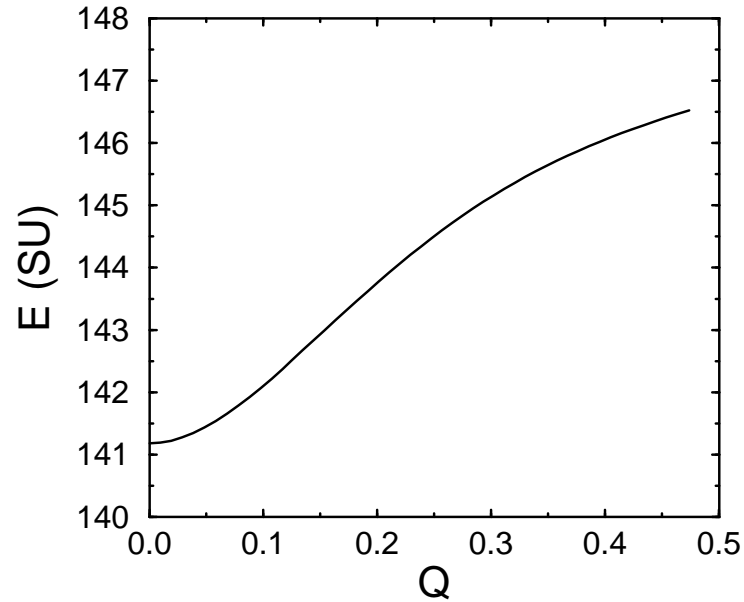


Figure 9: The potential energy for movement in the attractive channel, obtained by following the lowest mode. Q is defined in Eq. (34).

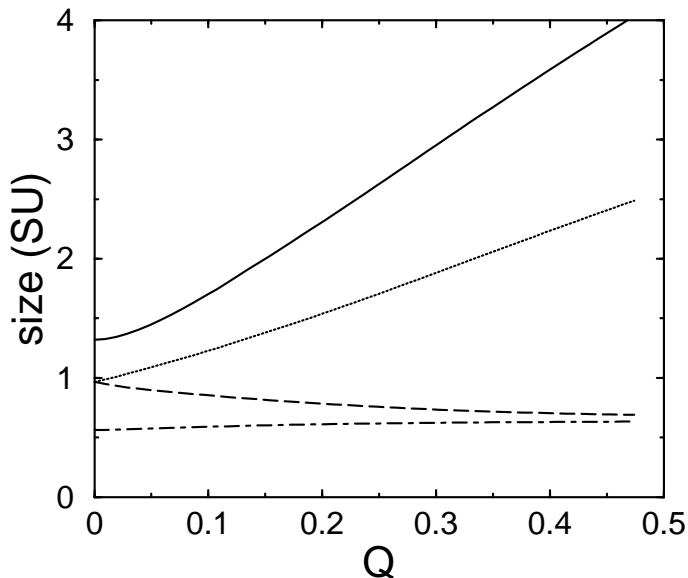


Figure 10: The size of the solution in three directions in the attractive channel, obtained by following the lowest mode. Q is defined in Eq. (34). The solid line gives R , the dotted curve is $\overline{hx^2i}$, the dashed curve $\overline{hy^2i}$, and the dash-dotted curve $\overline{hx^2i}$.

Note that we have defined Q such that the mass is exactly 1 so this parameter does not play a role here.

In Fig. 10 we show the size of the solution. We also exhibit the coordinate R , defined in Eq. (21). This can be used to remap all result in terms of this coordinate. In particular, one finds that $M(R) = (dQ/dR)^2$, all other quantities being scalars.

5.2 The hedgehog and the hedgehog-hedgehog channel

Let us first study the hedgehog solutions, to see whether there is a way out of the dilemma that the hedgehog is not connected to the hedgehog channel. As expected we find two sets of three negative energy modes, one of which corresponds to the hedgehog coming apart by an isorotation of the individual hedgehogs, and the other to the fission of the hedgehog into two hedgehogs. Since we have three axes, both sets of modes are threefold degenerate. In our numerical work following one of the fissioning modes, we had problems due to a mode that appeared spurious for the hedgehog (and was thus discarded), which becomes non-spurious for finite separation. Similar things always occur when we approach a state where an additional symmetry is realized, such as in nuclear physics, if we approach a state of axial symmetry [36]. In these cases the RPA frequency has a well defined limit as one approaches symmetry, since B and V

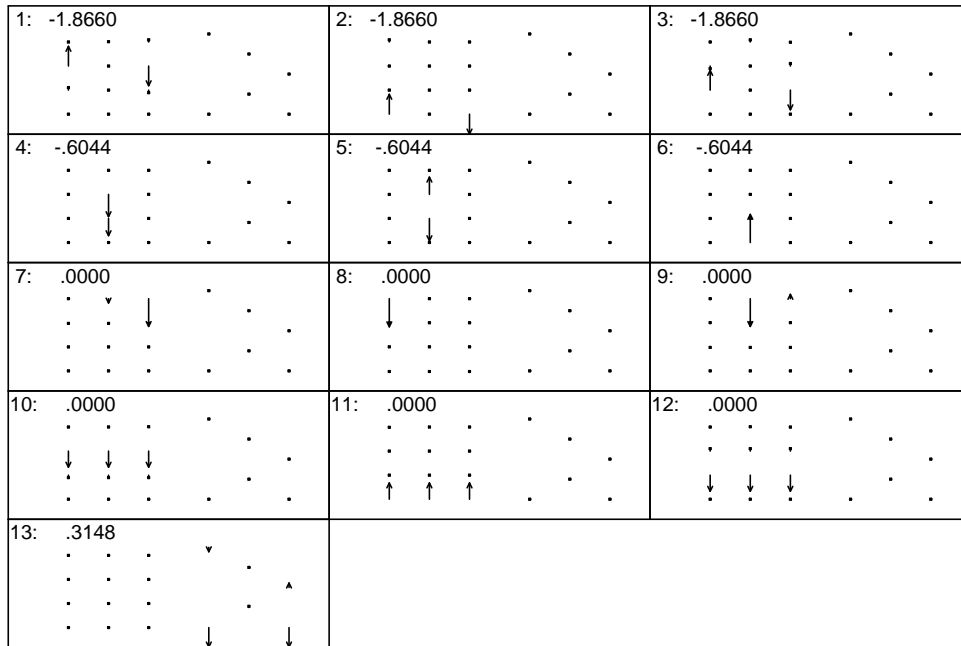


Figure 11: A schematic representations of the eigenvectors of the RPA problem around the $B = 2$ hedgehog. The arrows in the box denote the direction of change of the given component of the eigenvector. The four rows of three points in the left half of the box denote from bottom to top, the x , y and z components, with the upper line giving the change in ρ_i . The two uneven rows on the right denote the change in ρ (lower) and T (upper). We have also indicated the squares of the harmonic frequencies.

(short-hand for the covariant second derivative of V) approach zero at the same rate. Since the harmonic frequency is the square root of $V=B$, we cannot have that V is finite while B goes to zero. Actually as discussed in great detail in appendix B, this case is exactly realized in our numerical calculations! We find it hard to believe that the Skyrme model itself is so pathological, so we must assume that this is a problem of the AM Ansatz. That we do not see a way to smoothly connect the pole configuration in the hedgehog-hedgehog channel to the hedgehog is probably closely tied to this problem. It is worrisome and probably signifies that for strongly interacting Skyrme systems at small distances we should not take the AM Ansatz to be the final word. For the NN force this may not be so important, since the Skyrme model itself is suspect at these distances.

Studying the hedgehog channel is no major problem. The technique we used is to start with a pole configuration obtained from the "turning-point approach" discussed in Sec. 2 and iterate until convergence. At the point thus obtained we follow the relevant mode in both directions to obtain a picture of this channel. Fortunately the initial guess was quite close to the actual path.

Some of the results are presented in Figs. 12-15. In Fig. 12 we exhibit the inertial parameters for rotations, isorotations and translations (i.e., the mass) as a function of the coordinate Q . Since the configurations have axial symmetry around the axis of separation (x -axis) the yy and zz components of all these tensors are equal. The mass is almost constant since the energy is almost constant, and the breaking of Galilei invariance remains a minor nuisance. The moment of inertia for rotations increases drastically as Q increases, for rotations orthogonal to the axis of separation (x -axis). Parallel to this axis it decreases as expected.

There is quite some structure in the off-diagonal terms. The inertia for ordinary rotations around the x -axis is identical to that for isorotations around the same axis, whereas the mixing term is the opposite of these values. This of course shows that the states are invariant under the action of simultaneous rotations and isorotations along this axis. Quantum mechanically this implies that there can be no dynamical motion along this axis, and thus no kinetic energy proportional to $(L_x + J_x)^2$. Furthermore there is an (identical) off-diagonal term connecting the y and z components of rotations and isorotations.

In Fig. 13 we show the decoupling parameter D , defined in Eq. (38). This parameter is extremely small everywhere, showing excellent decoupling, i.e., one coordinate is enough to describe the dynamics in this channel. The small discontinuity near $Q = \pm 1$ is probably due to some solutions that are slightly less well converged than at the neighboring points. This is of course of no relevance, since the discontinuity in D is so small.

In Fig. 14 we show the potential energy V form overent in the hedgehog-hedgehog channel. This shows the expected repulsion in this channel. Note that the energy of the $B = 2$ hedgehog is 219.8 MeV, considerably higher than what we have reached in

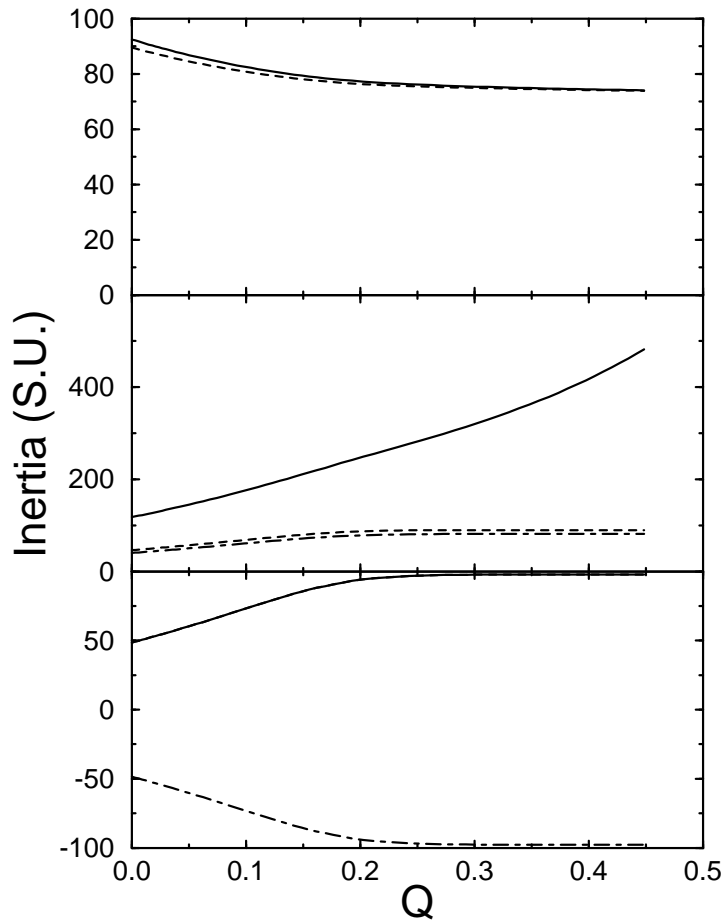


Figure 12: The inertial parameters in the hedgehog-hedgehog channel, obtained by following the lowest mode with the relevant symmetries. The lower two panels show the x and the $y = z$ components of the (iso)rotational moments of inertia (from bottom to top). Here solid lines represent rotational moments of inertia, dashed lines isorotational and dashed-dotted lines the off-diagonal component of the inertia tensor coupling the two. The upper panel shows the translational mass. The solid lines give the xx -, the dashed lines the yy - and the dashed-dotted lines the zz -component. Any component of the zero-mode inertia tensor not shown is identically zero.

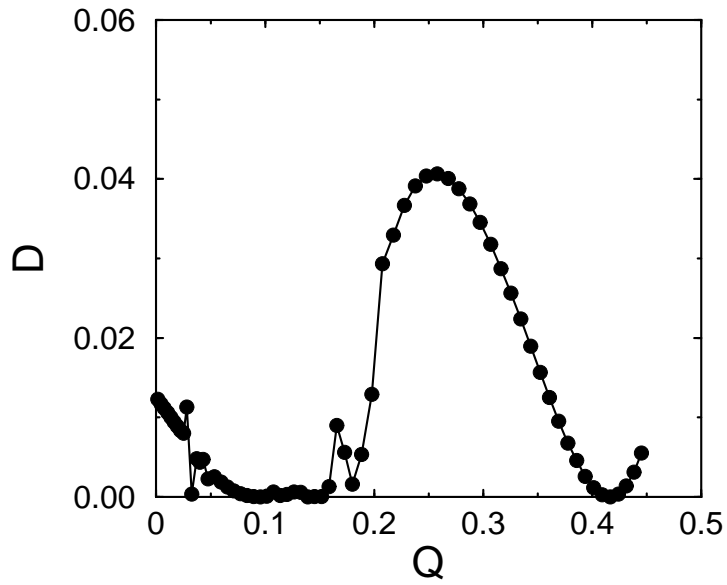


Figure 13: The decoupling measure D , Eq. (38), in the hedgehog-hedgehog channel, obtained by following the lowest mode with the correct symmetry.

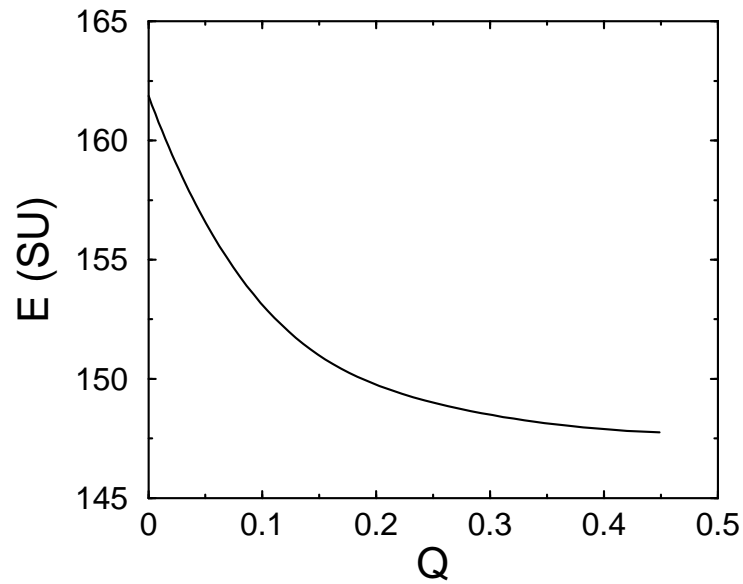


Figure 14: The potential energy for movement in the hedgehog-hedgehog channel, obtained by following the lowest mode.

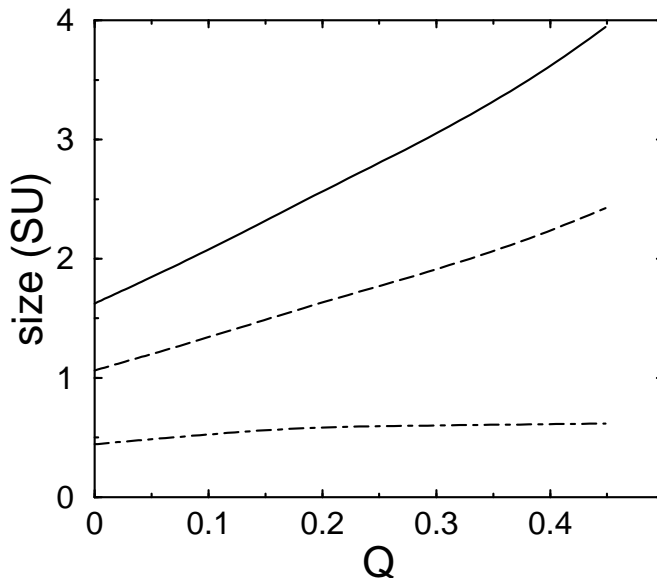


Figure 15: The size of the solution in three directions in the hedgehog-hedgehog channel, obtained by following the lowest mode. Q is defined in Eq. (34). The solid line gives R^2 , the dashed line $\langle hx^2 \rangle$, the dashed-dotted line $\langle hy^2 \rangle = \langle hz^2 \rangle$.

the current calculation.

In Fig. 15 we show the size of the solution. We also exhibit the coordinate R , defined in 21. One can see that the transverse size of the solution shrinks as R decreases.

5.3 The repulsive channel

A study of the repulsive channel appears to be more challenging. The first problem is to find the correct mode to start from. In order to find this solution we vary the parameter D , the size of the triangle, Eq. (20), for a given value of the parameter $\omega_2 = \omega = \tau$. For a suitably large value of τ (i.e., large separation) we then look for those values of D such that the valley conditions are satisfied. The problem arises that there are at least two solutions that look like they could evolve to a product Ansatz solution for large separation. We have followed both of them and rejected one which appears to evolve to a hedgehog that is too large. A further problem is that in this case the relevant mode is always the highest in RPA frequency. Since there is a mode that preserves the symmetry lower in the RPA spectrum, this violates the adiabatic assumption, and leads to instabilities. The other candidate appears to describe a solution that is better behaved. The hedgehogs seem a bit small, but we cannot follow to arbitrarily large separation.

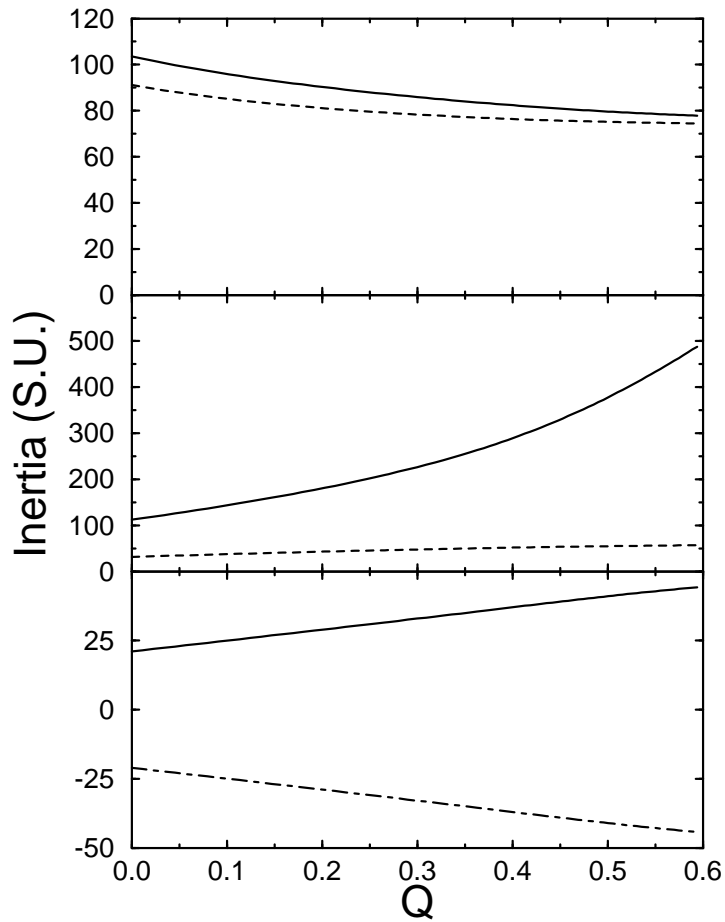


Figure 16: The inertial parameters in the repulsive channel, obtained by following the lowest mode. The lower two panels show the x and the $y = z$ components of the (iso)rotational moments of inertia (from bottom to top). Here solid lines represent rotational moments of inertia, dashed lines isotrotational and dashed-dotted lines the off-diagonal component of the inertia tensor coupling the two. The upper panel shows the translational mass. The solid lines give the xx -, the dashed lines the yy - and the dashed-dotted lines the zz -component. A xy component of the zero-mode inertia-tensor not shown is identically zero.

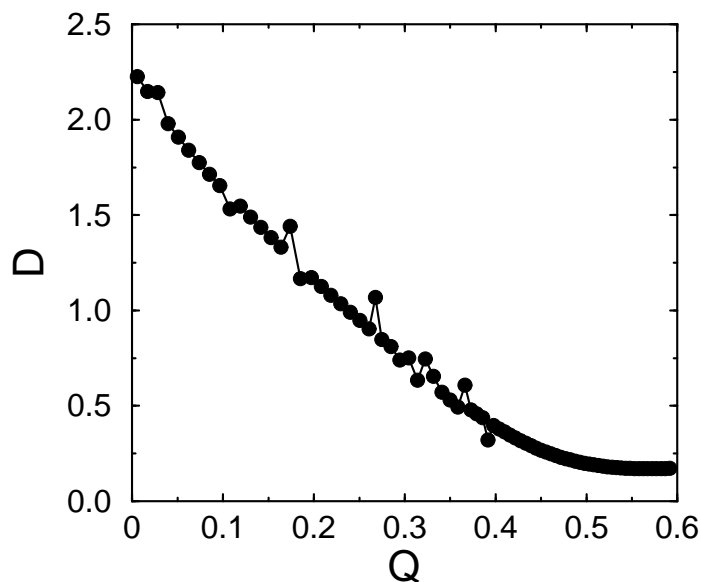


Figure 17: The decoupling measure D , Eq. (38), in the repulsive channel, obtained by following the lowest mode with the correct symmetry.

The inertia parameters, Fig. 16, show similar behavior as in the previous case. The inertia for ordinary rotations around the x -axis is identical to that for iso-rotations around the same axis, whereas the mixing term is the opposite of these values. Like in the hedgehog-hedgehog channel this implies the absence of terms of the form $(I_x + J_x)^2$ in the Hamiltonian. There are no further off-diagonal terms.

In Fig. 17 we show the decoupling parameter D . The decoupling measure is large, especially so at small separations. This indicates that a one-dimensional approach to the repulsive channel is not sufficient. There are two modes that contribute significantly to D . The manifold of these three modes corresponds exactly to the parametrization of Eq. (20). The one mode that preserves the reflection symmetries is always higher than the mode we follow, and the one that breaks the symmetry considerably lower in the spectrum (in most cases very close to zero, showing that the energy is almost flat in this direction), which has to do with being at a maximum of the energy (cf. Fig. 4). We should at least include all three these coordinates to get a reasonable result for a decoupled manifold, and thus for the collective Hamiltonian. The oscillations in D are due to problems to bring the solutions to convergence. For such a large decoupling measure, every minor flaw is amplified significantly.

In Fig. 18 we show the potential energy V for movement in the repulsive channel. The repulsion is indeed even stronger than in the hedgehog-hedgehog channel.

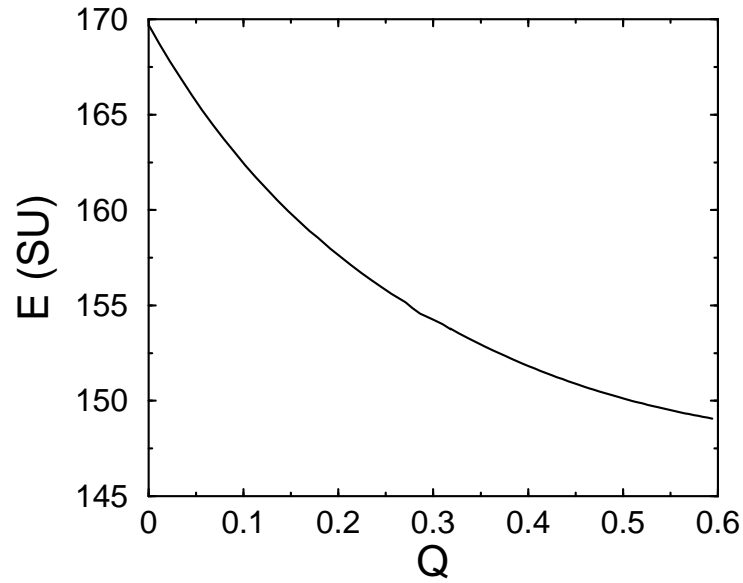


Figure 18: The potential energy for movement in the repulsive channel, obtained by following the lowest mode. Q is defined in Eq. (34)

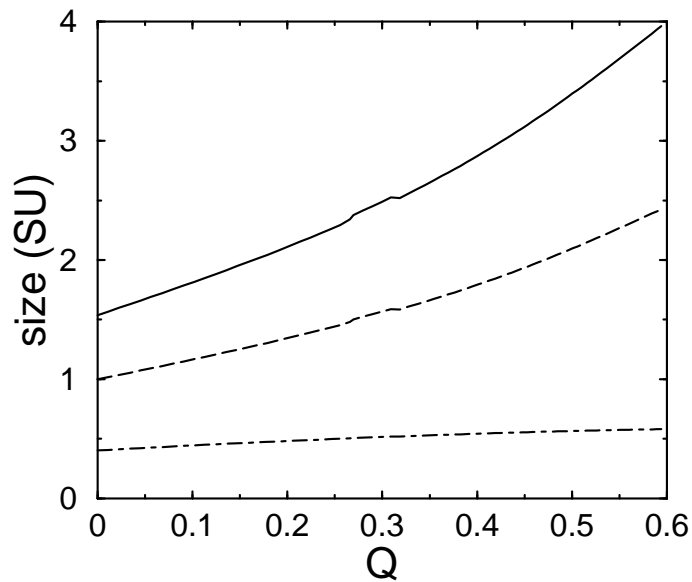


Figure 19: The size of the solution in three directions in the repulsive channel, obtained by following the lowest mode. Q is defined in Eq. (34). The solid line gives R , the dashed line $\langle x^2 \rangle$, the dashed-dotted line $\langle y^2 \rangle = \langle z^2 \rangle$.

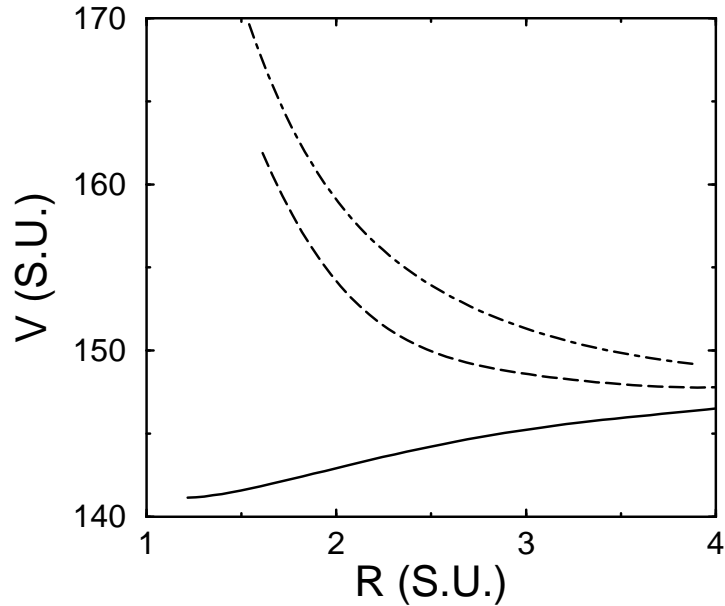


Figure 20: The potential energy as a function of R . The solid line gives the result for the attractive channel, dashed for the hedgehog-hedgehog channel, and dash-dotted for the repulsive channel.

5.4 NN projection

As discussed in great detail in Ref. [37] and Refs. [9, 10], one needs at least the three channels discussed here to project out a nucleon-nucleon force from the classical Skyrme ion-Skyrme ion interaction. The standard trick is to use the parametrization

$$V(\vec{R}) = v_1(R) + v_2(R)W + v_3(R)Z; \quad (35)$$

where W and Z take the values $1; 2, 1; 4$ and $3; 0$ in the attractive, repulsive and hedgehog-hedgehog channels, respectively. One then associates quantum operators with W and Z , which allows for the evaluation of a NN projection of V and by using the Born-Oppenheimer approximation, the NN force [10]. Of course this requires the identification of the coordinate R along the individual paths, which is probably incorrect. A more correct way would be to find the orthogonal geodesic lines that couple the points R on one path to the points R^0 on another, but this appears to be a very challenging task (if not outright impossible). We shall first convert the potentials presented previously to functions of R . In Fig. 20 these functions are shown. Of some interest is the size of the potential energy in the hedgehog channel, which is much lower than in the product Ansatz.

The mass in each channel is $(\frac{dR}{dq})^2$. In Fig. 21 we give in the attractive and hedgehog

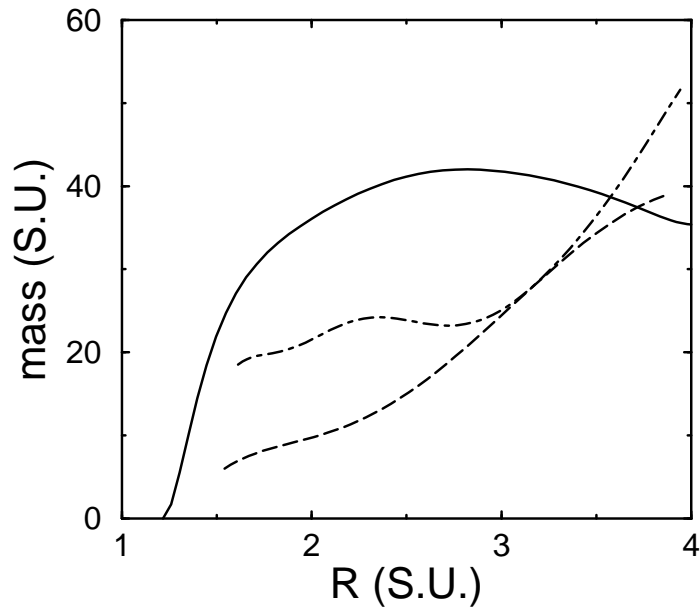


Figure 21: The mass as a function of R . The solid line gives the result for the attractive channel, dashed for the hedgehog-hedgehog channel, and dash-dotted for the repulsive channel.

channels this is a smooth function, which fact is of course closely related to the quality of decoupling. For large R the mass approaches the reduced mass for two hedgehogs, $36 S/U$. In the repulsive channel the behavior of the mass is surprising, but there decoupling is poor as well. One thus finds that the mass to be used in calculations is channel dependent, in a way similar to the potential energy.

6 Conclusions

It appears that the application of LACM techniques to the Skyrme model is a promising path in the study of the NN force. In this paper we have applied these techniques to the Aiyah-Manton ansatz, and obtained several interesting results. An analysis of the three standard "paths with reflection symmetries" yielded a wealth of information. One of the important aspects is that the results for the repulsive channel may not be reliable, since decoupling is poor. This should have an impact on the calculation of the nucleon-nucleon force from the Skyrme model, but we have not yet considered this aspect in the current paper. On the downside it appears that the AM ansatz has some undesirable problems (such as the lack of a consistent description of fluctuations around the $B = 2$ hedgehog). It would therefore be preferable to start from an Ansatz that is more fundamental than the ad-hoc form of the AM Ansatz.

One such route would be to apply the techniques of this paper to the Skyrme model defined on a grid, where the values of U at the grid points are the relevant dynamical variables. This would also allow for the addition of a (very physical) finite pion-mass term to the Lagrangian. The problem with such an approach is that, instead of a few discrete modes, one obtains a discretized approximation to bands of states (as in a solid). Only the band-heads are relevant for the discussion of LACM. The identification of the different bands is a complicated and highly non-trivial task. It may actually only be feasible for the channels discussed in this paper, where symmetries and their representations may be of some help in classifying the different phonon branches. Still one would like to be able to connect the different channels, through states without the additional symmetry, in order to obtain even more information about the geodesic structure of coordinate space (for a pedestrian: about the coordinate dependence of the kinetic energy).

Obviously we have not addressed in any detail the structure of the quantum Hamiltonian, and neither have we used all information derivable from the present calculation in the construction of the Hamiltonian. In Ref. [37] a boson model was used to analyze the finite N_c effective Hamiltonian for the spin and isospin rotational modes of the hedgehog. There one concentrated on the leading terms in the large N_c limit, which happens to be the potential energy. In order to make use of the results of the present paper one should extend the work of [37] to include information about the kinetic energy. One should then calculate the sub-leading terms in the large- N_c limit and match those on the ones calculated in the present work. Such an investigation is currently

underway. Due to the complexity of this task, this will be described in a separate paper.

Acknowledgments

The author wishes to acknowledge Dr. R. D. Amado and Dr. A. Klein for useful discussions, and Dr. R. Coombs for information about non-product formulas for integration, and sending us a copy of [38].

This work was supported in part by a grant from the Bundesministerium für Forschung und Technologie. The initial stages of the work, at the University of Pennsylvania, were supported by grants from the United States National Science Foundation and Department of Energy.

References

- [1] C. Holinde, R. Machleidt, and C. Elster, Phys. Rep. 149 (1987) 1.
- [2] G. 't Hooft, Nucl. Phys. B 72 (1974) 461.
- [3] E. Witten, Nucl. Phys. B 160 (1979) 57.
- [4] T. H. R. Skyrme, Nucl. Phys. 31 (1962) 556.
- [5] G. Adkins, C. Nappi, and E. Witten, Nucl. Phys. B 228 (1983) 552.
- [6] M. Lacombe, B. Loiseau, R. V. Mau, and W. N. Cottingham, Phys. Rev. Lett. 57 (1986) 170, and references therein.
- [7] A. Jackson, A. D. Jackson, and V. Pasquier, Nucl. Phys. A 432 (1985) 567.
- [8] J. K. Perring and T. H. R. Skyrme, Nucl. Phys. 31 (1962) 550.
- [9] N. R. Walet, R. D. Amado, and A. Hosaka, Phys. Rev. Lett. 68 (1992) 3849.
- [10] N. R. Walet and R. D. Amado, Phys. Rev. C 47 (1993) 498.
- [11] D. O. Riska and K. Dannbom, Phys. Scripta 37 (1988) 7.
- [12] T. Otofujii et al., Phys. Lett. B 205 (1988) 145.
- [13] R. Amado, B. Shao, and N. R. Walet, Phys. Lett. B 314 (1993) 159.
- [14] R. Amado, B. Shao, and N. R. Walet, PLB 324 (1994) 467.
- [15] A. Abada, preprint LPN-94-01, hep-ph/9401341 (unpublished).

- [16] T . S . W alhout and J . W ambach, *Phys. Rev. Lett.* 67 (1991) 314.
- [17] M . F . A tiyah and N . S . M anton, *Phys. Lett. B* 222 (1989) 438.
- [18] A . H osaka, M . O ka, and R . D . A mado, *Nucl. Phys. A* 530 (1991) 507.
- [19] M . F . A tiyah and N . S . M anton, *Commun. Math. Phys.* 153 (1993) 391.
- [20] T . G isiger and M . P aran jape, preprint UDEM -LPN -TH -94-196, hep-ph/9404319 (unpublished).
- [21] A . K lein, N . R . W alet, and G . D . D ang, *Ann. Phys.* 208 (1991) 90.
- [22] G . E . B rown and I . Z ahed, *Phys. Rep.* 142 (1986) 1.
- [23] E . N yman and D . R iska, *Rept. Prog. Phys.* 53 (1990) 1137.
- [24] J . J . M . V erbaarschot, T . S . W alhout, J . W ambach, and H . W . W yld, *Nucl. Phys. A* 468 (1987) 520.
- [25] J . J . M . V erbaarschot, *Phys. Lett. B* 195 (1987) 235.
- [26] N . S . M anton, *Phys. Lett. B* 192 (1988) 177.
- [27] V . B . K opeliovic and B . E . S tem, *JETP Lett.* 45 (1987) 203.
- [28] T . S . W alhout and J . W ambach, *J. Mod. Phys. E* 1 (1993) 665.
- [29] R . J ackiw, C . N ohl, and C . R ebbi, *Phys. Rev. D* 15 (1977) 1642.
- [30] N . R . W alet, A . K lein, and G . D . D ang, *Phys. Rev. C* 43 (1991) 2254.
- [31] R . B rankin, I . G ladwell, and L . S hampine, RK SU ITE : a suite of Runge-Kutta codes for the initial value problem for ODEs, Softreport 92-S1, Department of Mathematics, Southern Methodist University, Dallas, Texas, U.S.A (1992).
- [32] A . H . S troud, Approximate calculation of multiple integrals (Prentice Hall, Englewood Cliffs, 1971).
- [33] V . I . L ebedev, *Zh. vychisl. Mat. mat. Fiz.* 15 (1975) 48.
- [34] V . I . L ebedev, *Zh. vychisl. Mat. mat. Fiz.* 16 (1976) 293.
- [35] I . P . M ysovskikh, Interpolatory Cubature Formulas (in Russian) (Nauka, Moscow - Leningrad, 1981).
- [36] P . R ing and P . S chuck, The Nuclear Many-Body Problem (Springer, Berlin, 1980).

[37] M. Oka, R. Bijker, A. Bulgac, and R. D. Amado, Phys. Rev. C 36 (1987) 1727.

[38] R. Cools and P. Rabino witz, Monomial Cubature Rules since Stroud': A Compilation, Report TW 161, Department of Computing Science, Katholieke Universiteit Leuven, Leuven, Belgium (1994).

A Reflections and the product Ansatz

In this appendix we study those solutions of the Skyrme model in the $B = 2$ sector that have a simultaneous reflection symmetry in three orthogonal coordinate planes. To that end we assume that it is enough to determine what symmetries the product Ansatz has in the limit of large separations, and then require the same symmetry of any solution that evolves from it for finite separations. In this limit the U fields of the two individual baryon-one hedgehogs commute, and we can study the symmetries for a single hedgehog, or the relation of one hedgehog to the other, depending on the specific reflection plane.

The product Ansatz is defined by (we rotate one hedgehog by C and the other by C^Y , to obtain an initial form with maximal symmetry)

$$\begin{aligned} U_{PA}(\mathbf{x}; C) &= U U_+ = U(\mathbf{x}; R=2; C) U(\mathbf{x}; R=2; C^Y) \\ &= C [\cos f_+ + i\hat{x}_+ \sin f_+] C^Y [\cos f_+ + i\hat{x}_+ \sin f_+] : \end{aligned} \quad (36)$$

Here we use

$$f_+ = f(\mathbf{x}); \quad \mathbf{x}_+ = \mathbf{x} \cdot \frac{R}{2} \hat{e}_1 : \quad (37)$$

The function f is the chiral profile that describes the hedgehog.

For future use we introduce the rotation matrix $D = D[C]$ associated with C ,

$$D_{ij} = \frac{1}{2} \text{tr}[C_i C^Y_j] : \quad (38)$$

We write

$$D_{kl}^{(i)} = \delta_{kl} (1 - 2\delta_{ki}) : \quad (39)$$

for the diagonal matrix with one entry -1 , which describes a reflection in a coordinate plane. We are looking for those forms of the product Ansatz, where the field $U = u_4 + i\hat{x}_+ u$ after a reflection of the coordinate system in any of the three coordinate planes is related to itself by a coordinate independent transformation.

Let us first look at the \mathbf{x}_i , $i = 2; 3$. These transformations do not interchange the two hedgehogs, so that we can look for the symmetries of each hedgehog separately.

Explicitly we find, using Eq. (38),

$$\begin{aligned} U_+ &= \cos f_+ + i(D \hat{x}_+) \sin f \\ &= \cos f_+ + i(D^{(i)} \hat{x}_+) \sin f \end{aligned} \quad (40)$$

$$\begin{aligned} U &= \cos f + i(D^T \hat{x}) \sin f \\ &= \cos f + i(D^T (i) \hat{x}) \sin f \end{aligned} \quad (41)$$

We require that the components of U transform as

$$u^4 \rightarrow u^4; u \rightarrow S^{(i)} u; \quad (42)$$

where the matrix $S^{(i)}$ is constant. Under the remaining transformation $x_1 \rightarrow x_1$ we do interchange the two hedgehogs,

$$U_+ \rightarrow \cos f + i(D^{(1)} \hat{x}_+) \sin f \quad (43)$$

$$U \rightarrow \cos f_+ + i(D^T (1) \hat{x}_+) \sin f \quad (44)$$

Here we require the intertwining symmetry

$$u^4 \rightarrow u^4; u \rightarrow S^{(1)} u; \quad (45)$$

The symmetries lead to the conditions

$$\begin{aligned} S^{(i)} D &= D^{(i)}; \quad S^{(i)} D^T = D^T (i); \quad i=2;3; \\ S^{(1)} D &= D^T (1); \quad S^{(1)} D^T = D^{(1)}; \end{aligned} \quad (46)$$

These can be converted into equations for the S 's

$$\begin{aligned} S^{(i)} &= D^{(i)} D^T = D^T (i) D; \quad i=2;3; \\ S^{(1)} &= D^T (1) D^T = D^{(1)} D; \end{aligned} \quad (47)$$

Now let us see what these equations, which state that we have simultaneous symmetry under all three reflections, have to say about the matrix D . Equating the two forms for $S^{(i)}$ for $i=2;3$ leads to a condition on D^2 ,

$$(i) D^2 (i) = D^2; \quad (48)$$

The only type of matrix satisfying this condition for $i=2$ and 3 simultaneously is a diagonal matrix,

$$D^2 = \text{diag}(1; 1; 1); \quad (49)$$

with an even number of minus signs. Thus D^2 is either the identity or a rotation around any axis over an angle π . The only form for C allowed is then $C = \exp(i\frac{\pi}{2} \hat{n})$

with $\alpha = \frac{k}{2}$. The second of Eqs. (47) shows that $S^{(1)} = S^{(1)T}$. We need the following three conditions

$$\sin \hat{n}_1^2 \hat{n}_3 (1 - \cos \alpha) = 0; \quad (50)$$

$$\sin \hat{n}_1^2 \hat{n}_2 (1 - \cos \alpha) = 0; \quad (51)$$

$$\sin \hat{n}_1^2 \hat{n}_1 (1 - \cos \alpha) = \hat{n}_1 \sin \alpha; \quad (52)$$

There clearly exists the trivial solution for $\sin \alpha = 0$, or $\alpha = k$, with no restriction on \hat{n} . Two more interesting classes of solutions exist as well, where α can be any multiple of $\pi/2$

$$\hat{n} = (1; 0; 0); \hat{n} = (0; \cos \alpha; \sin \alpha); \quad (53)$$

Let us now calculate the matrices S for the interesting classes of solutions.

1. $\alpha = 0$: (HH-channel)

$$S^{(i)} = \delta^{(i)}; \quad (54)$$

2. $\hat{n} = (1; 0; 0)$, $\alpha = \pi/2$: (repulsive channel)

$$S^{(1)} = \text{diag}(1; 1; 1); \quad (55)$$

$$S^{(2)} = \text{diag}(1; 1; -1); \quad (56)$$

$$S^{(3)} = \text{diag}(1; -1; 1); \quad (57)$$

3. $\hat{n} = (0; \cos \alpha; \sin \alpha)$ ($\sin \alpha = 1$ only): (attractive channel)

$$S^{(1)} = \delta^{(1)}; \quad (58)$$

$$S^{(2)} = \begin{matrix} 0 & & & & 1 \\ \begin{matrix} \cos 2\alpha \\ 2 \cos^2 \alpha \sin \alpha \\ 2 \cos \alpha \sin^2 \alpha \end{matrix} & \begin{matrix} 2 \cos^2 \alpha \sin \alpha \\ 1 - 2 \cos^4 \alpha \\ 2 \cos^3 \alpha \sin \alpha \end{matrix} & \begin{matrix} 2 \cos \alpha \sin^2 \alpha \\ 2 \cos^3 \alpha \sin \alpha \\ \cos^4 \alpha + \sin^4 \alpha \end{matrix} & \begin{matrix} 1 \\ C \\ A \end{matrix} & \\ \end{matrix}; \quad (59)$$

$$S^{(3)} = \begin{matrix} 0 & & & & 1 \\ \begin{matrix} \cos 2\alpha \\ 2 \cos^2 \alpha \sin \alpha \\ 2 \cos \alpha \sin^2 \alpha \end{matrix} & \begin{matrix} 2 \cos^2 \alpha \sin \alpha \\ \cos^4 \alpha + \sin^4 \alpha \\ 2 \cos \alpha \sin^3 \alpha \end{matrix} & \begin{matrix} 2 \cos \alpha \sin^2 \alpha \\ 2 \cos \alpha \sin^3 \alpha \\ 1 + 4 \cos^2 \alpha \end{matrix} & \begin{matrix} 1 \\ C \\ A \end{matrix} & \\ \end{matrix}; \quad (60)$$

The standard reflection symmetries are usually taken to be the case $\alpha = 0$ and $\alpha = \pi/2$ with $\hat{n} = (1; 0; 0)$ and $(0; 0; 1)$. For this last unit vector we have

$$\begin{aligned} S^{(1)} &= \delta^{(1)}; \\ S^{(2)} &= \text{diag}(1; 1; 1); \\ S^{(3)} &= \text{diag}(1; 1; -1); \end{aligned} \quad (61)$$

B A naly sis of the behavior near the B = 2 hedgehog

Here we shall analyze the behavior of the mass matrix and the potential energy near the B = 2 hedgehog. Starting from

$$f(\mathbf{x};t) = \frac{1}{x^2 + (t - T)^2} + \frac{1}{x^2 + t^2} + \frac{1}{x^2 + (t + T)^2}; \quad (62)$$

we shall study the effect of changing the parameters T_i and T_i . The advantage of such a choice is that the matrix A_4 is Abelian, and for any change the U field is of hedgehog form,

$$U = \exp(i\vec{\alpha} \cdot \hat{x}(\mathbf{x})); \quad (63)$$

It is also not a restriction to study only this limited subset of modes, since in a numerical calculation we find that they decouple from the remaining modes.

To calculate the field it is only required to evaluate a simple integral,

$$\begin{aligned} \phi(\mathbf{x}) &= \int_{-1}^1 f(\mathbf{x};t) dt; \\ f(\mathbf{x};t) &= \partial_{x^2} \ln = \partial_{x^2} = : \end{aligned} \quad (64)$$

We shall use the subscript 0 to denote the default choice of JNR parameters of Eq. (62). If we now analyze the variations of f , we find that to lowest order

$$\begin{aligned} f &= f_0 + \frac{1}{0} \left(\frac{1}{x^2 + (t+T)^2} - \frac{1}{x^2 + (t-T)^2} \right) f_0 + \\ &\quad \left(\frac{2}{x^2 + t^2} - \frac{1}{x^2 + t^2} \right) f_0 + \\ &\quad \left(\frac{3}{x^2 + (t-T)^2} - \frac{1}{x^2 + (t-T)^2} \right) f_0 + \\ &\quad \left(\frac{2(t+T)T_1}{(x^2 + (t+T)^2)^2} - \frac{2}{x^2 + (t+T)^2} \right) f_0 + \\ &\quad \left(\frac{2tT_2}{(x^2 + t^2)^2} - \frac{2}{x^2 + t^2} \right) f_0 + \\ &\quad \left(\frac{2(t-T)T_3}{(x^2 + (t-T)^2)^2} - \frac{2}{x^2 + (t-T)^2} \right) f_0 : \end{aligned} \quad (65)$$

From this we can easily read off that there are four out of a total of six possible changes that leave f invariant. These are

1. $(T_1; T_2; T_3) = (1; 1; 1)$. In this case the three first terms inside the curly brackets combine to ∂_0 , and the three second terms combine to $\partial_0 f_0 = \partial_0$. These two contributions cancel. Of course this is the simultaneous rescaling of all three T_i 's, which is a zero mode for all pole configurations.

2. $(1; 0; 1) = (1; 0; 1)$. The reason here is time reversal invariance; thus

$$\int_{-\infty}^{\infty} \frac{1}{x^2 + (t+T)^2} - \frac{1}{x^2 + (t-T)^2} dt$$

is invariant under the interchange $T \rightarrow -T$, and the two contributions cancel.

3. $(0; 1; 0) = (0; 1; 0)$. The integrand is odd under the interchange $t \rightarrow -t$, and the integral vanishes.

4. $(1; 0; 1) = (1; 0; 1)$. The time-odd parts of the integrand give 0, and the two time-even parts cancel.

Of course the modes listed as 3 and 4 can be combined to the other trivial zero, a shift in the time-origin, which exists for all possible pole configurations. For the case of the hedgehog we are thus left with two additional unphysical modes, which are due to some residual gauge invariance [17], which is unbroken only for the particular choice of poles discussed here.

The mass matrix, which can be directly related to the first derivative of U w.r.t. the parameters must have zero eigenvalues in this space. It is not so obvious, and we shall argue also not true, that V has zero eigenvalues in the same subspace. If this were true we would feel happy discarding this part of the space, since no dynamical information is contained in these modes.

To study this problem we look at both B and V in the basis (components, in order, $1, 2, 3, T_1, T_2, T_3$)

$$\begin{aligned} e_1 &= \frac{1}{1+2} (1; 1; 1; 0; 0; 0); \\ e_2 &= \frac{1}{3} (0; 0; 0; 1; 1; 1); \\ e_3 &= \frac{1}{2} (1; 0; 1; 0; 0; 0); \\ e_4 &= \frac{1}{2+4} (1; 2; 1; 0; 0; 0); \\ e_5 &= \frac{1}{2} (0; 0; 0; 1; 0; 1); \\ e_6 &= \frac{1}{4} (0; 0; 0; 1; 2; 1); \end{aligned} \tag{66}$$

In this basis B and V have the six-by-six matrix form

$$B = \begin{pmatrix} 0 & 0 & 0 & 0 & 0 & 0 \\ 0 & 0 & 0 & 0 & 0 & 0 \\ 0 & 0 & 0 & 0 & 0 & 0 \\ 0 & 0 & 0 & 77.593 & 17.385 & 0 \\ 0 & 0 & 0 & 17.385 & 3.895 & 0 \\ 0 & 0 & 0 & 0 & 0 & 0 \end{pmatrix}; \quad (67)$$

$$V = \begin{pmatrix} 0 & 0 & 0 & 0 & 0 & 0 \\ 0 & 0 & 0 & 0 & 0 & 0 \\ 0 & 0 & 1.175 & 0 & 0 & .5474 \\ 0 & 0 & 0 & 24.176 & 5.426 & 0 \\ 0 & 0 & 0 & 5.426 & 1.212 & 0 \\ 0 & 0 & .5474 & 0 & 0 & .2464 \end{pmatrix}; \quad (68)$$

If one compares these two matrices, the problem is obvious: the two-by-two block spanned by the third and sixth vector is zero for B (as we had argued before), but it is non-zero for V. Actually the V block has one zero eigenvalue, but there is one eigenvector with infinite harmonic frequency ($\omega^2 = V=B$)! In the numerical calculations we see this eigenvalue coming down to finite values as we move away from the hedgehog. We believe that this pathology has nothing to do with the Skyrme model, but is caused by the Ansatz. The other two-by-two block (fourth and fifth components) has an eigenvalue very close to zero, but the same eigenvector and eigenvalue appears both in V and B. This reflects the fact that the chiral profile is, for large μ and T, approximately a function of $\mu = T^2$. This is only troublesome for numerical calculations, and causes no theoretical problems.

C Self consistent solutions in 1D LACM

Suppose we start from a point ϕ_0 where

$$V_i(\phi_0) = \mu_1 f_i^1(\phi_0); \quad (69)$$

$$V_{i,j}(\phi_0) B_{j,k}(\phi_0) f_k(\phi_0) = (\mu_1(\phi_0))^2 f_i(\phi_0); \quad (70)$$

are simultaneously satisfied. We could also calculate the left eigenvectors g_j of the RPA matrix, which we assume to be normalized as

$$g_j f_j = 1; \quad (71)$$

We now crank by adding g_{j_1} multiplied by a small number to ϕ_0 to obtain a new point ϕ_1 where these equations are not longer satisfied. More specifically,

$$V_i(\phi_1) = \sum_{j=1}^N \mu_j f_j(\phi_1); \quad (72)$$

$$V_{; ;} (1) B (1) f_{; } (1) = (!^{(1)})^2 f_{; } (1); \quad (73)$$

where we assume that by taking a small step from a point where the equations are satisfied, we have ϵ_1 .

(This last condition is only schematic. Since ϵ form the components of a vector, we should require that

$$B^{11} \epsilon_1^2 = B \epsilon^2; \quad (74)$$

Here we have used the fact that B is diagonal.)

Using a linear approximation to the first derivative of V ,

$$V_{; } (1 + \epsilon) = V_{; } (1) + V_{; ;} (1) \epsilon; \quad (75)$$

and assuming that the RPA eigenvectors do not change (which is not right, but iterative use of our update algorithm should be able to correct for this), we find that the choice

$$V_{; ;} (1) = \sum_{i=2}^N f_{; } (1) \quad (76)$$

will lead to a point where the desired equations are satisfied. (We have neglected one set of first order contributions, originating in the change of the eigenvector f^1 . This corresponds to assuming that the derivative of the RPA matrix is 0.) Let us now try to simplify the solution to (76) as much as possible:

$$V_{; ;} B = \sum_{i=2}^N f_{; } (!^{(1)})^2 g_{; } i; \quad (77)$$

$$B (V_{; ;}^{-1}) = \sum_{i=2}^N f_{; } (!^{(1)})^2 g_{; } i; \quad (78)$$

$$\begin{aligned} (V_{; ;}^{-1}) &= \sum_{i=2}^N B^{-1} f_{; } (!^{(1)})^2 g_{; } \\ &= \sum_{i=2}^N B^{-1} g_{; } (!^{(1)})^2 g_{; } \\ &= \sum_{i=2}^N g_{; } (V^{-1}) g_{; } \\ &= \sum_{i=2}^N g_{; } (V^{-1}) g_{; } : \end{aligned} \quad (79)$$

Here we have used the fact that in practice V is diagonal (in general we can always make a choice of basis such that this happens). If we now use $(1) = V_{; } g_{; }$, we have

$$\begin{aligned} &= \sum_{i=2}^N \sum_{j=2}^N g_{; } (V^{-1}) g_{; } f_{; } \\ &= \sum_{i=2}^N g_{; } (V^{-1}) g_{; } \\ &= \sum_{i=2}^N g_{; } (V^{-1}) g_{; } V_{; } : \end{aligned} \quad (80)$$